AIP Advances

RESEARCH ARTICLE | APRIL 05 2024

The effect of substrate-induced defects on structural and resistive switching properties in $Gd_{0.2}Ca_{0.8}MnO_3$ thin films

I. Angervo; A. Antola; A. Schulman; H. Huhtinen; P. Paturi

AIP Advances 14, 045309 (2024)
https://doi.org/10.1063/5.0185499

09 April 2024 06:34:17

AIP Advances ARTICLE pubs.aip.org/aip/adv

The effect of substrate-induced defects on structural and resistive switching properties in $Gd_{0.2}Ca_{0.8}MnO_3$ thin films

Cite as: AIP Advances 14, 045309 (2024); doi: 10.1063/5.0185499
Submitted: 23 February 2024 • Accepted: 14 March 2024 •
Published Online: 5 April 2024

View Online
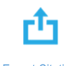
Export Citation

CrossMark

I. Angervo,[a] A. Antola, A. Schulman,[b] H. Huhtinen, and P. Paturi

AFFILIATIONS

Wihuri Physical Laboratory, Department of Physics and Astronomy, University of Turku, 20014 Turku, Finland

[a] **Author to whom correspondence should be addressed:** ijange@utu.fi
[b] **Current address:** Facultad de Ciencias, University of Salamanca, 37008 Salamanca, Spain

ABSTRACT

$Gd_{0.2}Ca_{0.8}MnO_3$ thin films were deposited on various substrate materials and their structural and resistive switching (RS) properties were investigated. The deposition resulted in epitaxial and polycrystalline films, with the latter also exhibiting distorted film surfaces. Both epitaxial and a part of polycrystalline films used as RS devices showed consistent RS performance in which an order of magnitude, or higher, switching ratios were achieved between high and low resistance states. The devices showed strong endurance during repeated switching cycles. However, under retention characterization, the resistance states did not remain distinguishable in devices constructed on polycrystalline films, while other devices maintained separable resistance states. The RS results are discussed in relation to the structural characteristics of the films, and this work helps us understand the RS mechanisms that still remain elusive in manganite-based devices.

© *2024 Author(s). All article content, except where otherwise noted, is licensed under a Creative Commons Attribution (CC BY) license (https://creativecommons.org/licenses/by/4.0/).* https://doi.org/10.1063/5.0185499

09 April 2024 06:34:17

I. INTRODUCTION

The resistive switching (RS) mechanism has attracted considerable interest for possible future consumer applications, such as resistance random access memory (RRAM) technology and neuromorphic computing.[1,2] RRAM is a non-volatile memory that can be switched between at least two resistance states, making it a potential candidate for next-generation memory devices. RRAM could be a potential breakthrough in neuromorphic computing hardware solutions,[2,3] which are designed to mimic the functionality of the human brain. Neuromorphic computing has the potential to overcome the limitations of current von Neumann architectures, which are based on the separation of memory and processing units. Integrating and designing the memory and processing unit into a singular device allows faster and more energy efficient computation. In artificial neural network grids, this is partly realized by transforming memory and logic into synaptic weights, effectively removing the need for the bus between memory and processing units. More generally, a non-volatile memristor device acting as a logic device, potentially replacing a transistor-based system, will ideally maintain its logic state once the state is set, reducing power consumption. Additionally, efficient matrix arithmetic can be achieved by utilizing a grid design, enabling parallel computation of matrix multiplication. Memristors exhibiting spike time dependent plasticity also play a pivotal role in implementing learning rules in neuromorphic hardware solutions.[4] Due to the stochastic nature of the RS, the phenomenon could be harnessed as a random number generator for security purposes.[5] All of this demonstrates the vast potential of future RS applications.

The RS mechanism has been confirmed in a wide variety of materials, but it has attracted particular interest in manganite and other perovskite systems, like $Pr_{1-x}Ca_xMnO_3$ (PCMO), $La_{1-x}Sr_xMnO_3$ (LSMO), and $SrTiO_3$ (STO).[6–9] However, in our previous studies, we have reported on promising results in $Gd_{1-x}Ca_xMnO_3$ based junctions.[10] Among other interesting results, we reported on the unexpected optimal RS ratio that can be obtained with high Ca substitution. This finding is at odds with other reports for other manganites regarding electron doping.[11,12] This in part

© Author(s) 2024

demonstrates the need for further research in order to understand the underlying mechanisms, to understand the differences between *a priori* similar compounds, and to realize the full potential of manganites as RS applications.

The RS and its mechanisms have been studied[11–22] and reviewed[7,8,23–25] for manganites and other oxides. The phenomenon is versatile, and the physical principles vary between materials. In PCMO, LSMO and other transition metal oxide (TMO)-based systems, the electrochemical migration of oxygen vacancies between TMO and the acting electrode is commonly addressed as a crucial factor in RS.[12–17,19,20] However, the detailed physical mechanisms remain inconclusive.

On the other hand, it is a well-established fact that structural stress or other deformation of the lattice can have a profound influence on the intrinsic properties of manganites,[26–29] particularly in thin film form. Structural stress and defects and their influence on manganites obviously account for a host of aspects, but one argument on this is the alteration of Mn–O–Mn bond angles, providing a direct influence on conductive properties. With respect to intrinsic properties, the RS properties cannot be detached from the microstructural attributes of an acting manganite/TMO electrode. Indeed, oxygen vacancy migration is likely to influence the material strain[14,21,30] and give rise to structural deformation.[19,31] Since dislocations in manganite can act as diffusion channels for oxygen vacancies,[32] the switching dynamic is expected to be altered by dislocations.[33,34] Regarding the practical research aspects, the structural defects can be engineered with manganite thin film substrate material.[35,36]

Here, we report on a comprehensive study of the RS mechanism in $Gd_{0.2}Ca_{0.8}MnO_3$ (GCMO)-based memristive devices on various substrate materials. This is performed in part to address the usability of substrates for GCMO films and to study the impact of strain and defects caused by the substrates on RS. Particularly, we apply the film deposition to Si and Si-based substrates. A successful thin film deposition preserving RS functionalities on Si wafers, which today's information technology relies on, provides a considerable advantage in upscaling any device for use in real-world applications.

II. EXPERIMENTAL DETAILS

A set of $Gd_{0.2}Ca_{0.8}MnO_3$ thin films was pulsed laser deposited on single crystal $SrTiO_3$ (STO), MgO, $NdGaO_3$ (NGO), and Si substrates. The films were also deposited on Si substrates with polycrystalline (Si-STO) and epitaxial $SrTiO_3$ (Si-STO-epi) buffer layers provided by Lumiphase. GCMO films are labeled and identified hereafter according to the substrate material. The deposition was performed at 700 °C in an oxygen atmosphere with 1500 pulses, resulting in a film thickness of ~80 nm.[37] However, the thickness may vary between different substrates. Gold pads with a 200 nm thickness for ohmic wire contacts were fabricated with a high vacuum electron beam deposition system provided by Elettrorava.

X-ray diffraction measurements were carried out using a PANalytical Empyrean diffractometer with a five axis goniometer and an Empyrean Cu LFF x-ray tube. Filtering the x rays with the BraggHD monochromator resulted in x rays consisting of only Cu $K_{\alpha1}/K_{\alpha2}$ components with minor traces of K_{β}. The measurements

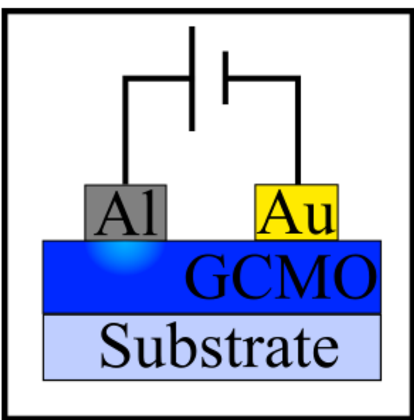

FIG. 1. Schematic image of the device design used for resistive measurements.

included θ–2θ scans between 10° and 130°, ϕ–ψ scan texture measurements for GCMO (204) ($2\theta = 60.81°$), 2θ–ϕ and 2θ–ω scans for GCMO (204) and (224) ($2\theta = 71.43°$). Apreo scanning electron microscope (SEM) provided by Thermo Fisher Scientific was utilized for structural thin film surface characterization.

Resistive characteristics were measured with a Keithley 2614b source-meter unit and with an ArC ONE memristor characterization platform. The measurements included $I(V)$ loops with 0 V → 7 V → −4 V → 0 V sequence and corresponding $R_{\text{probe}}(V)$ measurements with 0.4 V probe voltage. For more thorough quality monitoring, resistive switching endurance and retention measurements were performed with ArcONE. The planar devices were constructed by making contacts with an ultrasonic wire bonder using 33 μm diameter Al wire to Au pads and directly on top of the GCMO film. An ohmic contact is formed between Al wire and Au pad and between Au and GCMO.[10] The schematic of the device design is presented in Fig. 1.

III. RESULTS

A. Structural film properties

1. Crystallographical properties

The literature reference for crystallographic information is based on previous studies.[38] The x-ray diffraction θ–2θ measurements are presented for STO, Si-STO, and Si-STO-epi samples in Fig. 2(a) and for MgO, NGO, and Si in Fig. 2(b). The results presented in Fig. 2(a) show distinctive diffraction patterns for GCMO (00l) peaks for STO and Si-STO-epi, along with the corresponding substrate diffraction patterns. The peaks in Fig. 2(a) are labeled according to pseudo-cubic crystal symmetry. In addition, Si-STO-epi revealed a combination of two GCMO phases, as demonstrated in Fig. 2(a) inset. Other results presented in both Figs. 2(a) and 2(b) do not show pronounced peaks from GCMO. However, minor diffraction details can be identified as (011) and (002) GCMO peaks. A fully texturized GCMO phase was only confirmed in STO and Si-STO-epi; other samples indicate polycrystalline film growth. In NGO, the overlap between the substrate and GCMO peaks is immediate. For this reason, an accurate determination of peak attributes is

09 April 2024 06:34:17

© Author(s) 2024

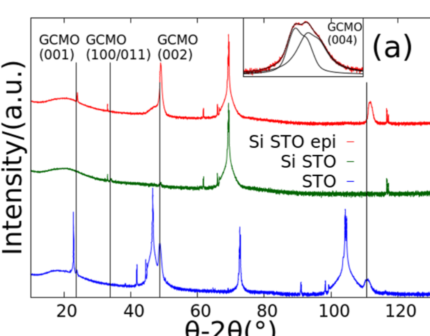

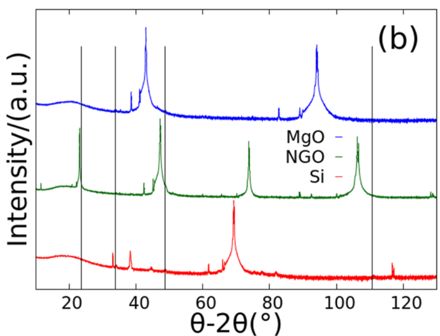

FIG. 2. (a) $\theta - 2\theta-$ results for STO, Si-STO, and Si-STO-epi, and (b) for MgO, NGO, and Si. Epitaxial GCMO growth is seen in STO and Si-STO-epi. Si-STO-epi reveals two distinctive GCMO phases, which is demonstrated by the double peak structure seen in (a) inset. Black lines indicate the corresponding peak positions for bulk GCMO.

TABLE I. The lattice parameter values obtained from XRD. Strain values are calculated based on the literature (Ref. 38).

Sample	a (Å)	b (Å)	c (Å)	V_{unit} (Å^3)	ε_a (%)	ε_b (%)	ε_c (%)
STO	5.338	5.288	7.486	212.3	0.72	0.14	0.35
Si-STO-epi$_1$	5.330	5.291	7.462	210.5	0.56	0.19	0.03
Si-STO-epi$_2$	5.332	5.330	7.434	211.3	0.60	0.93	−0.35

TABLE II. Peak broadening for STO and Si-STO-epi. The values correspond to full width half maximum values obtained from the Gaussian profile.

Sample	$\Delta\Phi_{204}$ (deg)	$\Delta\Phi_{224}$ (deg)	$\Delta\omega_{204}$ (deg)	$\Delta\omega_{224}$ (deg)
STO	0.74	0.94	0.74	1.29
STO-epi$_1$	0.69	0.94	0.68	1.25

impractical. The pronounced shoulder of GCMO (002) in Fig. 2(b) and the peak halo in 2D measurements suggest a texturized GCMO phase. However, the absence of the GCMO (004) peak, without significant overlap with the substrate peak, combined with the minor trace from GCMO (011) could be an indication of a significant polycrystalline phase.

Further structural analysis was made for both STO and Si-STO-epi, where the epitaxial growth and difference from the substrate peaks allow the determination of the parameters. c and a/b parameters were calculated using the Nelson–Riley method and by applying Bragg's law for GCMO (204) and (224) peak 2θ positions. The peak positions were obtained by fitting the pseudo-Voigt function to (00l) peaks and the 2D Gaussian function to (204) and (224) 2θ–ϕ results. Corresponding strain values ε_c and $\varepsilon_{a/b}$ for c and a/b parameters were calculated using a literature reference (Sarkar *et al.*[38]) for strain-free parameters and according to the formula $\varepsilon = (l - l_s)/l_s$, where l refers to the calculated lattice parameter and l_s to the strain-free reference parameter. These results are presented in Table I. The split GCMO phase was identified in (004) and (002) peaks, and lattice parameters/strains were obtained for both phases. In Table II, $\Delta\Phi$ and $\Delta\omega$ refer to the full width half maximum (FWHM) of the corresponding diffraction direction.

The results for FWHM and unit cell volume do not reveal any significant difference between STO and Si-STO-epi. The lattice parameters compared with reference values reveal tensile or compressive strain according to the same parameters, except for the c parameter in the secondary Si-STO-epi phase. Somewhat significant differences between GCMO phases in Si-STO-epi lattice parameters are an indication of nonuniform crystal growth. This could be explained by the fact that the STO buffer layer does not provide a uniform growth setting.

2. Microstructure of the films

The topography of the GCMO samples was studied with SEM. The results for 5 μm scans are presented in Fig. 3. It can be seen that the surfaces of NGO (c), Si-STO (d), Si (e), and MgO (f) have many cracks. These defects seem less pronounced in NGO and MgO, although the defects are still clear, extending roughly 1 μm in length. Linked cracks in Si and Si-STO extend over the 5 μm image size. This kind of structural deterioration in *in situ* films could obviously be a serious obstacle if μm-scale lithography is included in device fabrication.

STO (a) and Si-STO-epi (b) have uniform surfaces without any clear defects, as seen in the rest of the samples. Si-STO-epi appears to have a smooth surface without particular details outside of a few circular droplets. In STO, the surface appears more irregular compared to Si-STO-epi. The surface contains small particles that are less than 100 nm in diameter. The particles seem to stand on a smooth background surface, like in Si-STO-epi, and their number varies depending on measurement location. Otherwise, all the presented SEM results for each sample showed little to no variation from the rest of the data.

09 April 2024 06:34:17

© Author(s) 2024

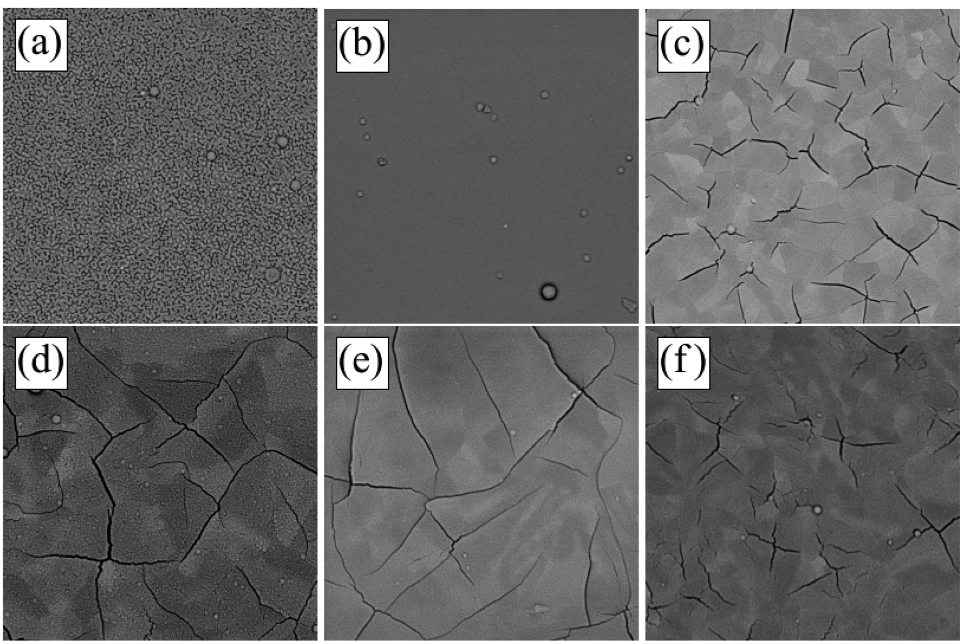

FIG. 3. The results obtained with scanning electron microscope for (a) STO, (b) Si-STO-epi, (c) NGO, (d) Si-STO, (e) Si, and (f) MgO.

09 April 2024 06:34:17

B. Resistive switching properties

The first resistive characterization was performed for four practically identical junctions in each film. An illustration of $R(V)$ loops (red) and respective probed loops (blue) is presented in Figs. 4(a)–4(d) for STO, MgO, NGO, and Si-STO-epi, respectively. All the presented results demonstrate a hysteretic asymmetric reversible resistance change with respect to the applied voltage. This is characteristic of bipolar resistive switching, which we have already demonstrated in our previous research for GCMO on STO substrates.[10] These results were obtained for all four devices on STO and MgO. The rest of the samples showed more inconsistent results between similar junctions or no proper performance at all. Si-STO-epi shows reversible resistance states in three out of four junctions, and two out of four junctions in NGO show promising performance, although a clear drift in switching states can be detected in the latter. Notably, the results in Fig. 4(e) for Si-STO showed practically no switching, resembling the results in Figs. 4(a)–4(d). Although some results, as depicted in Fig. 4(f), obtained for Si do indicate hysteretic resistance change, consistency between junctions and between scans in the same junction is poor. It is concluded that no resistive switching was detected in Si-STO with the current measurements and with the current device design, and due to poor performance in Si, the two samples are disregarded from the rest of the discussion.

For a more detailed analysis, high resistance (HRS) and low resistance states (LRS) were extracted from $R_{\text{probe}}(V)$ results. The states were obtained as probed resistance values after 0 V. The results are presented for STO, MgO, NGO, and Si-STO-epi in Figs. 5(a)–5(d), respectively. The results are scaled according to the median LRS for each junction. LRS and HRS states can be distinguished in all cases for STO, MgO, and Si-STO-epi. The results demonstrate that STO and MgO show maximum switching close to two orders of magnitude. Si-STO-epi switching is below one order of magnitude. However, in NGO, the HRS and LRS states overlap. In the $R_{\text{probe}}(V)$, this was apparent due to significant drift in the resistance, while a single scan still showed distinguishable LRS and HRS.

Additionally, we found that RESET switching takes place at a localized, practically identical voltage, close to −0.4 V, in all the samples. SET switching showed considerable variation between devices on different substrates but also between junctions on the same substrate and between measurements for the same junction. However, SET switching was well-localized, close to 3.5 V for MgO. On STO, Si-STO-epi, and NGO, the junctions showed more gradual transitions to LRS. This indicates that the microstructure plays a more prominent role in the SET process and that a more controlled fabrication process could mitigate the dispersion observed in the junctions of the same substrate.

In order to harvest resistive switching functionalities in applications, reliable devices are required. For this, we studied the endurance and retention measurements of the devices, as those are fundamental properties that all non-volatile memory devices must possess. An example of the endurance and retention results is presented in Figs. 6(a) and 6(b) for STO. The combined results for all samples are presented in (c) for endurance and in (d) for retention measurements. These results are normalized according to the lower resistance state median in order to improve clarification. The combined endurance data reveals that all the samples show well-separated and local resistance states throughout the endurance

© Author(s) 2024

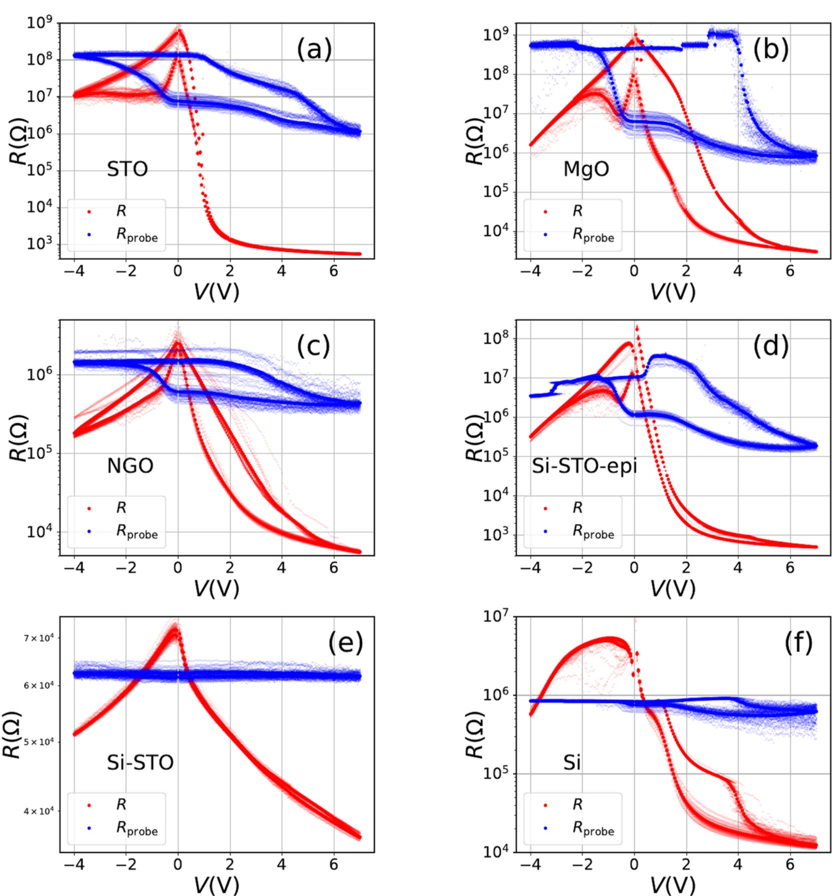

FIG. 4. Resistive switching characterization for (a) STO, (b) MgO, (c) NGO, (d) Si-STO-epi, (e) Si-STO, and (f) Si present resistance (red) and probed resistance (blue) between 7 and −4 V, demonstrating hysteretic multi-state resistance with looped voltage. Opaque points show the average of multiple loops. A single loop is shown with transparent points.

09 April 2024 06:34:17

sequence. A striking detail from the data shows that in Si-STO-epi 7.0 V, the write pulse sets the junction into a lower resistance state, while in the other samples, the pulse results in a high resistance state. In the combined retention results, it becomes clear that only STO and Si-STO-epi LRS and HRS states remain distinguishable. However, the polarity in Si-STO-epi is again reversed compared to endurance results. Additional measurements revealed that Si-STO-epi exhibits an unstable switching state that relaxes after the writing pulse. Once the delay between the writing pulse and the reading pulse is extended to ∼1 s, the endurance measurements show stable LRS and HRS states in which LRS is reached by applying a 7.0 V voltage pulse.

IV. EFFECT OF FILM GROWTH AND STRUCTURAL DEFECTS IN THE SWITCHING MECHANISMS

Figure 7 illustrates the following discussion topics in RS and structural characteristics. In Sec. III B, we have demonstrated significant structural differences in GCMO films deposited on various substrates. These differences can be summarized by two sample groups: polycrystalline samples with deteriorated film surfaces and epitaxial samples with uniform film surfaces. These structural characteristics link to RS performance by showing consistent bipolar switching, consistent switching in endurance tests, and distinctive LRS and HRS in retention measurements in the latter group. In the group, including polycrystalline samples and/or deteriorated film surfaces, MgO and NGO show bipolar switching endurance, but LRS and HRS do not remain distinctive under retention, while other samples do not reveal proper RS characteristics at all.

Interfacial modification by oxygen vacancy migration is usually seen as a contributor to RS in multiple materials. Structural defects can induce local variation in vacancy concentration and, hence, variation in conductivity,[39] which again could mean variations in local switching in the junction area.[13] Since our samples have shown clear differences in structural characteristics, it could be expected that devices on different substrates perform differently under RS characterization. In addition, with the current device design, junction size and the acting interface remain somewhat uncontrollable.

© Author(s) 2024

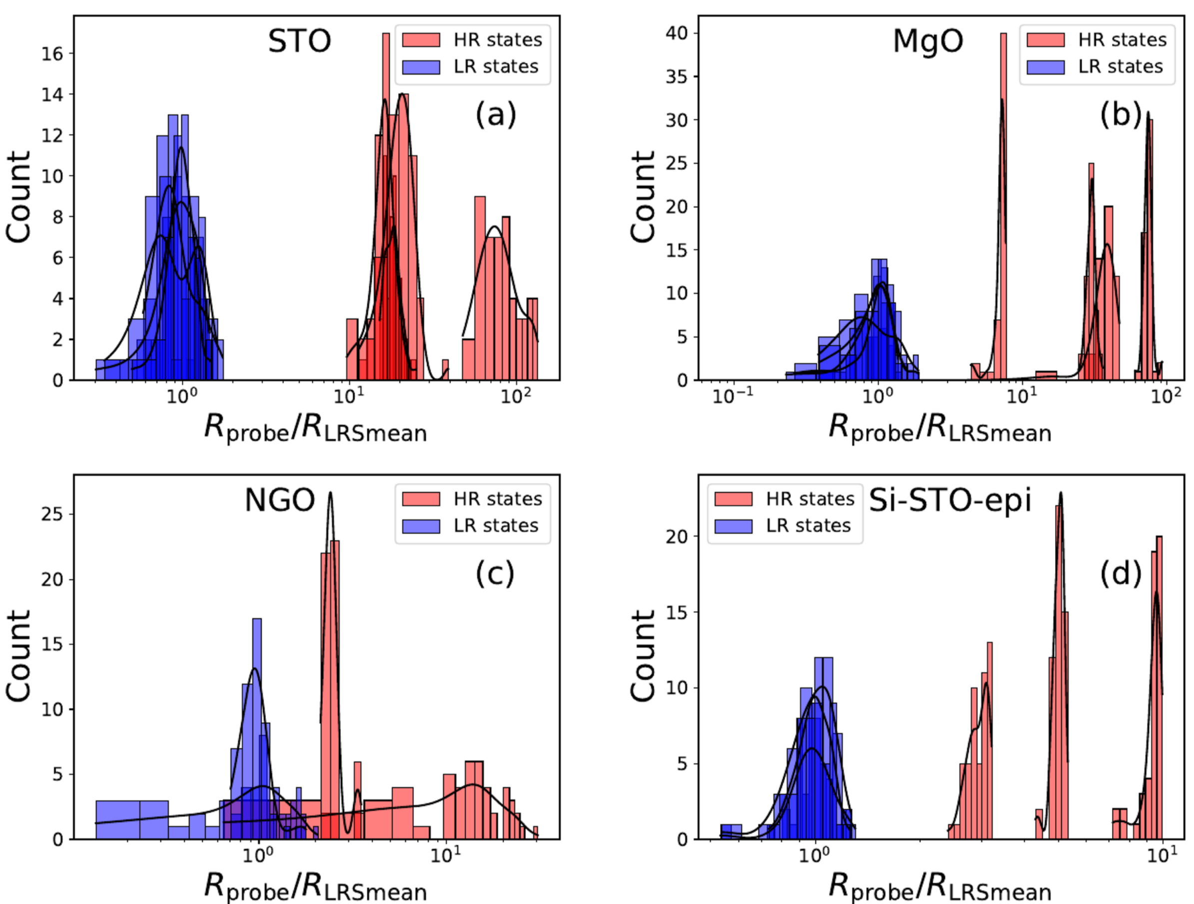

FIG. 5. Collected results from probed resistance results for all devices corresponding to HRS and LRS obtained at 0 V for (a) STO, (b) MgO, (c) NGO, and (d) Si-STO-epi.

09 April 2024 06:34:17

Previous research on manganites demonstrates that both epitaxial and non-epitaxial systems show RS performance.[3,12,17,22,33,40–44] This is also our observation here for GCMO-based devices. Indeed, comparing epitaxial STO and polycrystalline MgO in RS performance, the results show clear switching between distinctive LRS and HRS, as depicted in Figs. 5(a) and 5(b). In addition, the endurance of these states shows that repeated switching shows only little variation in resistive states. Perhaps the most remarkable difference between the two samples is the lack of retention in MgO, while STO preserves the distinction between LRS and HRS. The relaxation of LRS toward HRS has been demonstrated in many systems, and it could mean oxygen vacancy diffusion or the detrapping of charge carriers in the vicinity of the interface.[43,45,46] It is possible that in a manganite, the structural defects, like grain boundaries, act as diffusion channels for oxygen[32] and hence likely prompt RS but possibly also cause LRS "leaking" into more stable HRS through diffusion. It is worth noting that multiple publications address the role of dislocations in resistive switching.[39,47,48] Since all our polycrystalline samples have also indicated clear dislocations or cracks in the film surface, it is easy to suggest that diffusion is more pronounced in the polycrystalline samples and, hence, LRS states cannot be distinguished from HRS throughout the retention characterization.

The differences in SET/RESET processes could also be attributed to differences in oxygen migration dynamics. Figuratively, the localized SET/RESET switching in MgO in the RS measurements seems to suggest that oxygen vacancies are highly mobile between the two states once a threshold voltage is surpassed and, hence, the device switches to the final state with only a little voltage increase. However, with other samples, especially, SET switching happens more gradually.

In order to further discuss the underlying principles that result in RS performance, we note that while oxygen vacancy migration in manganites is regarded as the key to understanding the phenomenon, this conclusion does not address the underlying principles in detail. One elaborate remark has been the modification of the PCMO bandgap in the vicinity of the active electrode. The electrical stimulus has been argued to modify a Schottky-like barrier, therefore resulting in the respective LRS and HRS.[12] Acknowledging

© Author(s) 2024

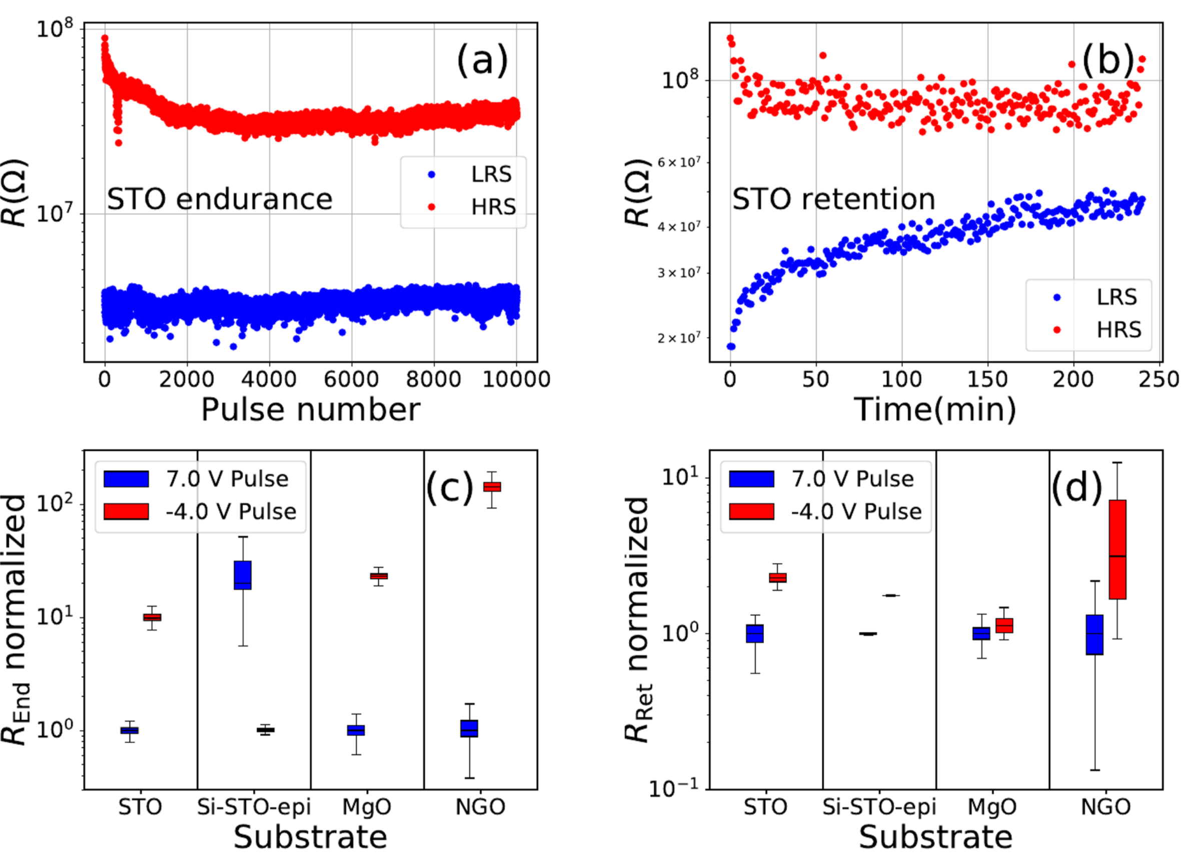

FIG. 6. Endurance (a) and retention (b) results for STO. Combined endurance (c) and retention (d) results for devices that showed resistive switching. The results in (c) and (d) are normalized according to the lower resistance state median for clarification.

09 April 2024 06:34:17

the role of oxygen vacancy migration, an explanation emphasizing the role of a malleable oxide tunnel barrier with filament-like conduction at the active interface has also been provided.[20] While the RS is regularly argued to be an interface phenomenon, the movement of oxygen during the SET/RESET process can create trapping sites in manganite bulk, thus contributing to the RS.[49] Although it is difficult and potentially incorrect to pinpoint a single factor responsible for RS in our manganite system, the previous research seems to suggest that while oxygen migration is likely the key actor, its effects could be an interplay of multiple mechanisms.

Finally, we discuss the results and the differences between STO and Si-STO-epi, both showing an epitaxial GCMO phase. The structural differences between the two are somewhat subtle, but Si-STO-epi revealed a double GCMO phase with different strain values and a smoother GCMO surface. Oxygen migration has been demonstrated to include structural deformation of the crystal lattice,[19,30,31] and structural stress has been argued to influence or correlate with the oxygen migration.[14,16] On top of all, local structural transition-based RS, excluding oxygen migration, has also been proposed.[50] Considering these remarks, it could have been predicted that Si-STO-epi, showing two GCMO phases with distinctive strain values, would demonstrate more anomalous RS characteristics. This was evident and demonstrated in Fig. 5, in which the SET/RESET process was accompanied by irregular characteristics. In addition, Si-STO-epi showed volatile, reversed switching characteristics in endurance measurements. Reversed RS polarity has been demonstrated in earlier research[51,52] and argued to result from coexisting RS mechanisms, including oxygen vacancy migration and electron trapping at the interface region.[51] Although the remarks about possible double mechanisms in RS in Si-STO-epi will remain speculative, the decaying RS with reversed polarity suggests a more complicated switching scheme in which RS becomes clouded with decaying resistance states.

Our new research builds upon newly discovered resistive switching in GCMO systems. Especially the choice of substrate material demonstrates the versatility and malleability of the phenomenon. In addition, further research will provide a deeper understanding of the unexpected results and role of structural defects in resistive switching. One improvement for the current research

© Author(s) 2024

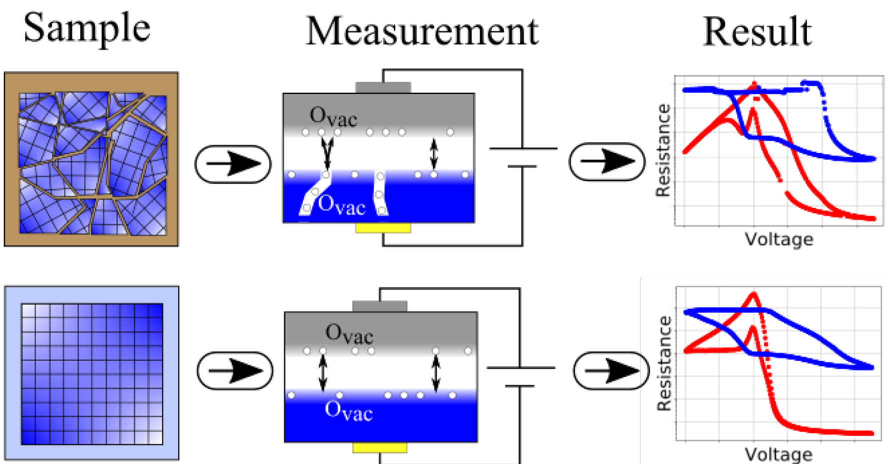

FIG. 7. Schematic representation of the discussion topics, regarding the results obtained for GCMO devices demonstrating structural differences and resistive switching.

would be accomplished with capacitive devices, providing a more controlled device design and cutting down variations between technically identical devices.

V. CONCLUSIONS

In this work, we have demonstrated resistive switching in GCMO films deposited on various substrates. Epitaxial GCMO systems show consistent switching. While part of the polycrystalline samples failed to show reliable switching, the epitaxial crystal structure is not a prerequisite for the phenomenon. However, the differences in resistive switching between samples have been linked and discussed according to detected microstructural changes. In particular, STO and STO buffered silicon were utilized as successful substrates in obtaining epitaxial GCMO phases. Respective resistive switching characteristics, on the other hand, were distinctive and probably linked to more anomalous crystal characteristics indicated in the GCMO phase deposited on buffered silicon.

ACKNOWLEDGMENTS

Jenny and Antti Wihuri Foundation, Academy of Finland, Business Finland Foundation, Finnish Cultural Foundation (Grant No. 00230224), and the University of Turku Graduate School UTUGS are acknowledged for financial support.

AUTHOR DECLARATIONS

Conflict of Interest

P. Paturi, A. Schulman, and H. Huhtinen have Patents FI20205101 (31.1.2020), PCT/FI2021/050057 (29.1.2021), TW110103063 (27.1.2021)

Author Contributions

I. Angervo: Formal analysis (equal); Investigation (equal); Writing – original draft (equal). **A. Antola**: Writing – review & editing (equal). **A. Schulman**: Conceptualization (equal); Writing – review & editing (lead). **H. Huhtinen**: Conceptualization (equal); Writing – review & editing (equal). **P. Paturi**: Conceptualization (equal); Supervision (equal); Writing – review & editing (equal).

DATA AVAILABILITY

The data that support the findings of this study are available from the corresponding author upon reasonable request.

REFERENCES

[1] I. Baek, M. Lee, S. Seo, M. Lee, D. Seo, D.-S. Suh, J. Park, S. Park, H. Kim, I. Yoo, U.-I. Chung, and J. Moon, Tech. Dig. IEDM, 2004.
[2] D. Ielmini, Microelectron. Eng. **190**, 44 (2018).
[3] S. Park, J. Noh, M. l. Choo, A. M. Sheri, M. Chang, Y.-B. Kim, C. J. Kim, M. Jeon, B.-G. Lee, B. H. Lee, and H. Hwang, Nanotechnology **24**, 384009 (2013).
[4] M. Prezioso, M. Mahmoodi, F. M. Bayat, H. Nili, H. Kim, A. Vincent, and D. Strukov, Nat. Commun. **9**, 5311 (2018).
[5] H. Jiang, D. Belkin, S. E. Savelev, S. Lin, Z. Wang, Y. Li, S. Joshi, R. Midya, C. Li, M. Rao, M. Barnell, Q. Wu, J. J. Yang, and Q. Xia, Nat. Commun. **8**, 882 (2017).
[6] S. Bagdzevicius, K. Maas, M. Boudard, and M. Burriel, J. Electroceram. **39**, 157 (2017).
[7] A. Sawa, Mater. Today **11**, 28 (2008).
[8] R. Waser, R. Dittmann, G. Staikov, and K. Szot, Adv. Mater. **21**, 2632 (2009).
[9] X. L. Hong, D. J. J. Loy, P. A. Dananjaya, F. Tan, C. W. Ng, and W. X. Lew, J. Mater. Sci. **53**, 8720 (2018).
[10] V. Lähteenlahti, A. Schulman, A. Beiranvand, H. Huhtinen, and P. Paturi, ACS Appl. Mater. Interfaces **13**, 18365 (2021).
[11] Y. Tokunaga, Y. Kaneko, J. P. He, T. Arima, A. Sawa, T. Fujii, M. Kawasaki, and Y. Tokura, Appl. Phys. Lett. **88**, 223507 (2006).
[12] S. Asanuma, H. Akoh, H. Yamada, and A. Sawa, Phys. Rev. B **80**, 235113 (2009).
[13] M. J. Rozenberg, M. J. Sánchez, R. Weht, C. Acha, F. Gomez-Marlasca, and P. Levy, Phys. Rev. B **81**, 115101 (2010).

09 April 2024 06:34:17

© Author(s) 2024

[14]Y. B. Nian, J. Strozier, N. J. Wu, X. Chen, and A. Ignatiev, Phys. Rev. Lett. **98**, 146403 (2007).
[15]D. S. Jeong, H. Schroeder, and R. Waser, Phys. Rev. B **79**, 195317 (2009).
[16]T. Kramer, M. Scherff, D. Mierwaldt, J. Hoffmann, and C. Jooss, Appl. Phys. Lett. **110**, 243502 (2017).
[17]F. Borgatti, C. Park, A. Herpers, F. Offi, R. Egoavil, Y. Yamashita, A. Yang, M. Kobata, K. Kobayashi, J. Verbeeck, G. Panaccione, and R. Dittmann, Nanoscale **5**, 3954 (2013).
[18]X. Chen, N. Wu, J. Strozier, and A. Ignatiev, Appl. Phys. Lett. **89**, 063507 (2006).
[19]Z. Liao, P. Gao, X. Bai, D. Chen, and J. Zhang, J. Appl. Phys. **111**, 114506 (2012).
[20]A. Herpers, C. Lenser, C. Park, F. Offi, F. Borgatti, G. Panaccione, S. Menzel, R. Waser, and R. Dittmann, Adv. Mater. **26**, 2730 (2014).
[21]K. Maas, E. Villepreux, D. Cooper, E. Salas-Colera, J. Rubio-Zuazo, G. R. Castro, O. Renault, C. Jimenez, H. Roussel, X. Mescot, Q. Rafhay, M. Boudard, and M. Burriel, Adv. Funct. Mater. **30**, 1909942 (2020).
[22]P. Solanki, M. Vala, D. Dhruv, S. V. Bhatt, and B. Kataria, Surf. Interfaces **35**, 102474 (2022).
[23]R. Waser and M. Aono, Nat. Mater. **6**, 833 (2007).
[24]W. Banerjee, R. D. Nikam, and H. Hwang, Appl. Phys. Lett. **120**, 060501 (2022).
[25]B. Sun, G. Zhou, L. Sun, H. Zhao, Y. Chen, F. Yang, Y. Zhao, and Q. Song, Nanoscale Horiz. **6**, 939 (2021).
[26]C. S. Nelson, J. P. Hill, D. Gibbs, M. Rajeswari, A. Biswas, S. Shinde, R. L. Greene, T. Venkatesan, A. J. Millis, F. Yokaichiya, C. Giles, D. Casa, C. T. Venkataraman, and T. Gog, J. Phys.: Condens. Matter **16**, 13 (2004).
[27]E. Dagotto, T. Hotta, and A. Moreo, Phys. Rep. **344**, 1 (2001).
[28]A.-M. Haghiri-Gosnet and J.-P. Renard, "CMR manganites: Physics, thin films and devices," J. Phys. D: Appl. Phys. **36**, R127 (2003).
[29]W. Prellier, P. Lecoeur, and B. Mercey, J. Phys.: Condens. Matter **13**, R915 (2001).
[30]S. Majumdar, H. Huhtinen, S. Granroth, and P. Paturi, J. Phys.: Condens. Matter **24**, 206002 (2012).
[31]C. Jooss, J. Hoffmann, J. Fladerer, M. Ehrhardt, T. Beetz, L. Wu, and Y. Zhu, Phys. Rev. B **77**, 132409 (2008).
[32]A. M. Saranya, D. Pla, A. Morata, A. Cavallaro, J. Canales-Vázquez, J. A. Kilner, M. Burriel, and A. Tarancón, Adv. Energy Mater. **5**, 1500377 (2015).
[33]N. Kanegami, Y. Nishi, and T. Kimoto, Appl. Phys. Lett. **116**, 013501 (2020).
[34]C. Park, S. H. Jeon, S. C. Chae, S. Han, B. H. Park, S. Seo, and D.-W. Kim, Appl. Phys. Lett. **93**, 042102 (2008).
[35]A. Herpers, K. J. O'Shea, D. A. MacLaren, M. Noyong, B. Rösgen, U. Simon, and R. Dittmann, APL Mater. **2**, 106106 (2014).
[36]M. Nyman, T. Elovaara, J. Tikkanen, S. Majumdar, H. Huhtinen, and P. Paturi, Phys. Procedia **75**, 1122 (2015).
[37]A. Beiranvand, M. O. Liedke, C. Haalisto, V. Lähteenlahti, A. Schulman, S. Granroth, H. Palonen, M. Butterling, A. Wagner, H. Huhtinen, and P. Paturi, J. Phys.: Condens. Matter **33**, 255803 (2021).
[38]B. Sarkar, R. Nag, and S. Pal, "Study of magnetic properties with temperature and field variation of electron doped $Ca_{0.85}Gd_{0.15}MnO_3$," Physica B **570**, 224 (2019).
[39]K. Szot, W. Speier, G. Bihlmayer, and R. Waser, Nat. Mater. **5**, 312 (2006).
[40]V. Lähteenlahti, A. Schulman, H. Huhtinen, and P. Paturi, J. Alloys Compd. **786**, 84 (2019).
[41]H. K. Lau, C. W. Leung, and Y. K. Chan, Phys. Status Solidi A **206**, 2182 (2009).
[42]X. Liu, K. P. Biju, E. M. Bourim, S. Park, W. Lee, J. Shin, and H. Hwang, Solid State Commun. **150**, 2231 (2010).
[43]S.-L. Li, D. S. Shang, J. Li, J. L. Gang, and D. N. Zheng, J. Appl. Phys. **105**, 033710 (2009).
[44]D.-J. Seong, J. Park, N. Lee, M. Hasan, S. Jung, H. Choi, J. Lee, M. Jo, W. Lee, S. Park, S. Kim, Y. H. Jang, Y. Lee, M. Sung, D. Kil, Y. Hwang, S. Chung, S. Hong, J. Roh, and H. Hwang, *2009 IEEE International Electron Devices Meeting* (IEEE, 2009), p. 1.
[45]M. Fujimoto, H. Koyama, Y. Nishi, and T. Suzuki, Appl. Phys. Lett. **91**, 223504 (2007).
[46]S. M. Sadaf, E. M. Bourim, X. Liu, S. H. Choudhury, D.-W. Kim, and H. Hwang, Appl. Phys. Lett. **100**, 113505 (2012).
[47]R. Muenstermann, T. Menke, R. Dittmann, S. Mi, C.-L. Jia, D. Park, and J. Mayer, J. Appl. Phys. **108**, 124504 (2010).
[48]C. Kalkert, J.-O. Krisponeit, M. Esseling, O. I. Lebedev, V. Moshnyaga, B. Damaschke, G. van Tendeloo, and K. Samwer, Appl. Phys. Lett. **99**, 132512 (2011).
[49]S. Lashkare, V. Saraswat, and U. Ganguly, ACS Appl. Electron. Mater. **2**, 2026 (2020).
[50]J.-O. Krisponeit, C. Kalkert, B. Damaschke, V. Moshnyaga, and K. Samwer, Phys. Rev. B **82**, 144440 (2010).
[51]M. Scherff, B. Meyer, J. Hoffmann, C. Jooss, M. Feuchter, and M. Kamlah, New J. Phys. **17**, 033011 (2015).
[52]K. Shibuy, R. Dittmann, S. Mi, and R. Waser, Adv. Mater. **22**, 411 (2010).

09 April 2024 06:34:17

© Author(s) 2024